The HL-LHC Low-β Quadrupole Magnet MQXF: from Short Models to Long Prototypes

P. Ferracin, G. Ambrosio, M. Anerella, H. Bajas, M. Bajko, B. Bordini, R. Bossert, N. Bourcey, D. W. Cheng, G. Chlachidze, L. Cooley, S. Ferradas Troitino, L. Fiscarelli, J. Fleiter, M. Guinchard, S. Izquierdo Bermudez, S. Krave, F. Lackner, F. Mangiarotti, M. Marchevsky, V. Marinozzi, J. Muratore, F. Nobrega, H. Pan, J.C. Perez, I. Pong, S. Prestemon, H. Prin, E. Ravaioli, G. Sabbi, J. Schmalzle, S. Sequeira Tavares, S. Stoynev, E. Todesco, G. Vallone, P. Wanderer, X. Wang, M. Yu

***Abstract*—Among the components to be upgraded in LHC interaction regions for the HiLumi-LHC projects are the inner triplet (or low-β) quadrupole magnets, denoted as Q1, Q2a, Q2b, and Q3. The new quadrupole magnets, called MQXF, are based on Nb_3Sn superconducting magnet technology and operate at a gradient of 132.6 T/m with a conductor peak field of 11.4 T. The Q1 and Q3 are composed by magnets (called MQXFA) fabricated by the US Accelerator Upgrade Project (AUP) with a magnetic length of 4.2 m. The Q2a and Q2b consists of magnets (called MQXFB) fabricated by CERN with a magnetic length of 7.15 m. After a series of short models, constructed in close collaboration by the US and CERN, the development program is now entering in the prototyping phase, with CERN on one side and BNL, FNAL, and LBNL on the other side assembling and testing their first long magnets. We provide in this paper a description of the status of the MQXF program, with a summary of the short model test results, including quench performance, and mechanics, and an update on the fabrication, assembly and test of the long prototypes.**

***Index Terms*— High Luminosity LHC, Interaction Regions, Low-β Quadrupoles, Nb3Sn magnets**

I. Introduction

In order to reduce the beam size by a factor two in the interaction points, and to increase the rate of collisions by a factor of five, the HL-LHC Project [1] is planning to install in the LHC Interaction Regions (IR) new inner triplet (or low-β) quadrupole magnets, called MQXF [2]-[6]. With respect to the current triplet quadrupole magnets, MQXF will feature a larger aperture, from 70 to 150 mm, a higher peak field, from 8.6 to 11.4 T, and a new superconducting material, Nb_3Sn instead of Nb-Ti. Out of the 30 triplets magnets (including spares) that will be installed in the HL-LHC, 20 magnets, called MQXFA and 4.2 m long, will be fabricated by the US Accelerator Research Program (AUP), a continuation of the LARP Program [7].

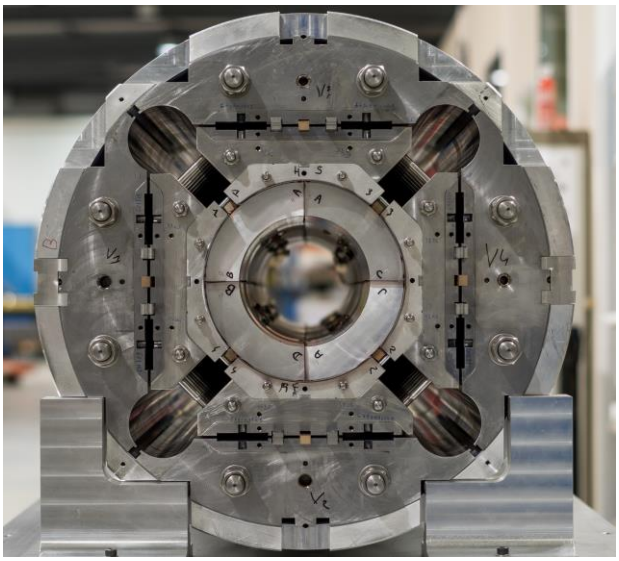

Fig. 1. A view of the MQXFS support structure with Al dummy coils.

The remaining 10 magnets, called MQXFB and 7.15 m long, will be fabricated by CERN. Both MQXFA and MQXFB, which have identical cross-sections and 3D design, will have to produce at a nominal gradient of 132.6 T. The fabrication of the so-called "series magnets", i.e. the ones to be installed in the machine, will start in 2019, and it was preceded by the development of short model magnets, 1.5 m long, and full-length prototypes, constructed and tested to characterized magnet performance. At the time of the submission of this paper, 4 short models (MQXFS1-3-5-4) and 2 MQXFA prototypes (MQXFAP1-2) have been tested, while the first MQXFB prototype (MQXFBP1) is being assembled. In addition, two single-coil tests, called MQXFSM1 and MQXFAM1 for the short and long coils, have been carried out. We provide here a description of the conductor and coils used in the different magnets, the preloading conditions, and a summary of the quench performance.

This work was supported by the U.S. Department of Energy, Office of Science, Office of High Energy Physics, through the US LHC Accelerator Research Program (LARP) and the US LHC Accelerator Upgrade Project (AUP), and by the High Luminosity LHC project at CERN.

P. Ferracin, H. Bajas, M. Bajko, B. Bordini, N. Bourcey, S. Ferradas Troitino, L. Fiscarelli, J. Fleiter, M. Guinchard, S. Izquierdo Bermudez, F. Lackner, F. Mangiarotti, J.C. Perez, H. Prin, E. Ravaioli, S. Sequeira Tavares, E. Todesco, G. Vallone, are with CERN, CH-1211 Geneva 23, Switzerland (e-mail: paolo.ferracin@cern.ch).

G. Ambrosio, R. Bossert, G. Chlachidze, S. Krave, V. Marinozzi, F. Nobrega, S. Stoynev, M. Yu are with Fermi National Accelerator Laboratory, Batavia, IL 80510 USA.

M. Anerella, J. Muratore, J. Schmalzle, P. Wanderer, are with BNL, Upton, NY 11973-5000, USA.

D. W. Cheng, M. Marchevsky, I. Pong, S. Prestemon, G. Sabbi, X. Wang, are with Lawrence Berkeley National Lab, Berkeley, CA 94720, USA.

L. D. Cooley is with the Applied Superconductivity Center, National High Magnetic Laboratory, Tallahassee, FL 32310, USA

II. Superconducting Strand and Cable

The MQXF coils are wound with a cable composed by 40 strands with a diameters of 0.85 mm. For all the MQXFA series magnets, RRP 108/127 strands from Bruker will be used. The same strand will be utilized for 8 of the 10 MQXFB series magnets, while in the remaining two Bruker's PIT 192 with bundle barrier will be used [8]. In addition to these two types of strands, the short models and the prototypes employed also different strand architectures, namely RRP 132/169, RRP 144/169, and PIT 192 (without bundle barrier). In Fig. 2, the strands' cross-sections are shown, while the strand specification are given in Table I. Both strands must have a critical current >331 A at 15 T, while a 7% lower critical current at 12 T was set for the PIT strand (>590 A instead of >632 A).

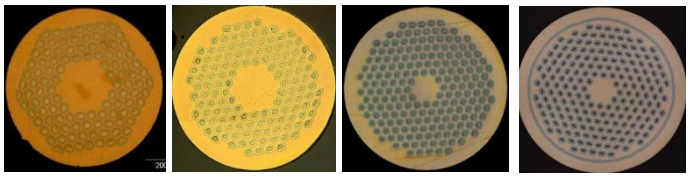

Fig. 2. Superconducting strands used for the MQXF program (left to right): RRP 108/127, RRP 132/169, PIT 192, PIT 192 with bundle barrier.

TABLE I
Strand Specifications

Parameter	Unit	RRP	PIT
Strand diameter	mm	0.85	
Sub-element diameter	µm	≤55	
Filament twist pitch	mm	19±3	
Cu/SC		1.2±0.1	
RRR		>150	
I_c (12 T, 4.2 K), no self-field corr.	A	>632	>590
I_c (15 T, 4.2 K), no self-field corr.	A	>331	>331
Non-Cu J_c (12 T, 4.2 K), no self-field corr.	A/mm^2	>2450	>2290
Non-Cu J_c (15 T, 4.2 K), no self-field corr.	A/mm^2	>1280	>1280

TABLE II
Cable Specifications

Parameter	Unit	
Number of strands in cable		40
Cable bare width (before/after HT)	mm	18.150/18.363
Cable bare mid-thick. (before/after HT)	mm	1.525/1.594
Cable bare inner-thick. (before/after HT)	mm	1.462/1.530
Cable bare outer-thick. (before/after HT)	mm	1.588/1.658
Cable width expansion during HT	%	1.2
Cable mid-thick. expansion during HT	%	4.5
Keystone angle	Deg.	0.40
Pitch length	mm	109
Cable core width	mm	12
Cable core thickness	µm	25
Cabling I_c degradation	%	<5
RRR after cabling		>100
Insulation thickness per side at 5 MPa	µm	145±5

The cable, whose parameters are given in Table II, is 18.150 mm wide, and it contains a 316L stainless steel core 25 µm thick to reduce dynamics effects during magnet ramping. Both the design of the coil fabrication tooling (in particular the curing/reaction/impregnation cavity size) and the coil cross-section have been defined assuming a cable expansion during heat treatment of 4.5% in thickness and 1.2% in width [9]. The critical current degradation due to cabling is set as <5%.

In Fig. 3 the strand critical current specifications, including self-field correction and 5% cabling degradation, are fitted with a parameterization curve [10] and compared with the magnet load-line (conductor peak field vs. magnet current). The short sample currents I_{ss}, which represents the magnet's current limits and are obtained from the intersection of the magnet load-line with the 1.9 K critical curves, are 21.26 kA for the RRP and 20.89 kA for the PIT. This means that, at the nominal current I_{nom} of 16.47 kA, the magnet will operate at a percentage of short sample of 77% (RRP) and 79% (PIT). Also, the according to the HL-LHC project requirements, the MQXF magnet must be able to reach an ultimate current I_{ult} 8% higher than I_{nom}, that is 20.89 kA. At this current, the percentages of I_{ss} are 84% (RRP) and 86% (PIT).

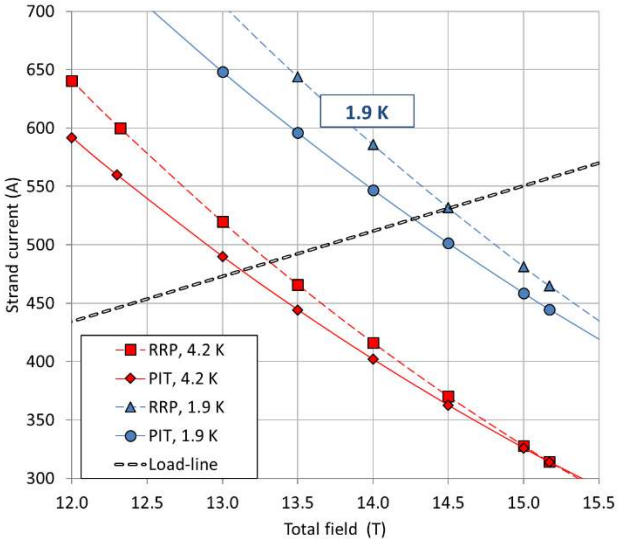

Fig. 3. Strand critical currents vs. total magnetic field (including self-field correction and 5% cabling degradation): specifications for RRP 108/127 and PIT 192 with bundle, and magnet load-line.

III. Coil Fabrication

Since the beginning of the development of the MQXF magnet, the fabrication of the coils has proceed in parallel in the US laboratories and at CERN [11]-[16]. Short model coils from US and CERN were identical, and therefore usable in the same magnet. Prototype and series coils are instead different in lengths, consistently to the magnetic lengths of MQXFA (4.2 m) and MQXFB (7.15 m). The main parameters of the coils implemented in MQXF magnets are given in Table III. Both short coils and MQXFA coils were fabricated using two different cable design: a 1st generation cable with keystone angle of 0.55°, and a 2nd generation cable, where the angle was decreased to 0.40° to reduce the critical current degradation due to cabling for both RRP and PIT strands. A second modification, which took place during the coil fabrication, was the increase of the magnetic length for MQXFA/B from 4.0/6.8 m to 4.2/7.15 m; the first MQXFA coils were still 4.0 m long.

TABLE III
PARAMETERS OF COIL USED IN SHORT MODELS AND PROTOTYPES

Coil	Laboratory[a]	Strand	Cross-section	L^b	Magnet
2	LARP/AUP	RRP 108/127	1st gen.	1.19	MQXFSM1
103	CERN	RRP 132/169	1st gen.	1.19	MQXFS1a-d
104	CERN	RRP 132/169	1st gen.	1.19	MQXFS1a-d
3	FNAL/BNL	RRP 108/127	1st gen.	1.19	MQXFS1a-d
5	FNAL/BNL	RRP 108/127	1st gen.	1.19	MQXFS1a-d
105	CERN	RRP 132/169	2nd gen.	1.20	MQXFS3a-c
106	CERN	RRP 132/169	2nd gen.	1.20	MQXFS3a-c
107	CERN	RRP 132/169	2nd gen.	1.20	MQXFS3a-c
7	FNAL	RRP 108/127	2nd gen.	1.20	MQXFS3a-b
8	FNAL/BNL	RRP 144/169	2nd gen.	1.20	MQXFS3c
203	CERN	PIT 192	2nd gen.	1.20	MQXFS5
204	CERN	PIT 192	2nd gen.	1.20	MQXFS5
205	CERN	PIT 192	2nd gen.	1.20	MQXFS5
206	CERN	PIT 192	2nd gen.	1.20	MQXFS5
108	CERN	RRP 108/127	2nd gen.	1.20	MQXFS4
109	CERN	RRP 108/127	2nd gen.	1.20	MQXFS4
110	CERN	RRP 108/127	2nd gen.	1.20	MQXFS4
111	CERN	RRP 108/127	2nd gen.	1.20	MQXFS4
QXFP01	FNAL/BNL	RRP 108/127	1st gen.	4.00	MQXFAM1
QXFP02	FNAL/BNL	RRP 132/169	1st gen.	4.00	MQXFAP1
QXFP03	FNAL	RRP 144/169	2nd gen.	4.00	MQXFAP1
QXFP04	FNAL/BNL	RRP 132/169	2nd gen.	4.00	MQXFAP1
QXFP05	FNAL	RRP 108/127	2nd gen.	4.00	MQXFAP1
QXFA102	FNAL	RRP 108/127	2nd gen.	4.20	MQXFAP2
QXFA104	FNAL/BNL	RRP 108/127	2nd gen.	4.20	MQXFAP2
QXFA105	FNAL	RRP 108/127	2nd gen.	4.20	MQXFAP2
QXFA106	FNAL/BNL	RRP 108/127	2nd gen.	4.20	MQXFAP2
104	CERN	RRP 108/127	2nd gen.	7.15	MQXFBP1
105	CERN	RRP 108/127	2nd gen.	7.15	MQXFBP1
107	CERN	RRP 108/127	2nd gen.	7.15	MQXFBP1
108	CERN	RRP 108/127	2nd gen.	7.15	MQXFBP1

[a]Laboratory where the coil was produced. The case "FNAL/BNL" refers to coils wound/cured at FNAL, and reacted/impregnated in BNL.
[b]Magnetic length (m).

A. Winding, Curing, Reaction, Impregnation

The MQXF coils are composed by 50 turns, wound in 2 layers around a Ti-alloy pole with a single unit length of cable (no internal splices). Each layer is divided in 2 blocks per quadrant. The coil winding is performed by keeping a tension on the cable of 25 kg. After the first layer is wound, polymer-derived ceramic binder CTD-1202 is applied to the S2 glass insulation of the cables; the layer is then cured in two steps, first at 80 °C for 2 h, then at 170 °C for 3 h. The same operation is applied to the second layer, after its winding on top of the first layer. Once the winding and curing is completed, the coil is placed in a reaction mold and heat treated in an oven under argon flow. The heat treatments are based on the following schedules: 48 h at 210 (ramp 25 °C/h), 48 h at 400 °C (ramp 50 °C/h), 50 h at 665 °C (ramp 50 °C/h) for the RRP, and 40 h at 415 °C, 120 h at 620 °C, 200 h at 645 °C (all with ramp 30 °C/h) for the PIT with bundle. Before transferring the reacted coil in the impregnation mold, printed circuits (traces) with quench heaters and voltage taps are placed on top of the outer layer and connected. At the same time, the splicing operation, consisting in soldering Nb-Ti cables to the Nb_3Sn coil leads, is executed. The impregnation process consists in inserting the coil, placed inside a dedicated mold, inside a vacuum tank, and injecting CTD-101K epoxy resin system at atmospheric pressure (MQXFA) or at 2 bar (MQXFB). The epoxy is injected with resin and mold at a temperature of 60 °C. The epoxy curing is done in two plateaus, the first at 110 °C for 6 h and the second at 125 °C for 16 h.

B. Coil Dimensional Measurements

Before the magnet assembly, coils dimensions are measured using a Coordinate Measurement Machine (CMM). Data are acquired on the outer radius and the mid-planes of the coils in different locations along the longitudinal direction [17]. By aligning the data on the nominal outer radius of the impregnated coil (113.376 mm), it is possible to estimate the deviations of the azimuthal dimensions with respect to the nominal values.

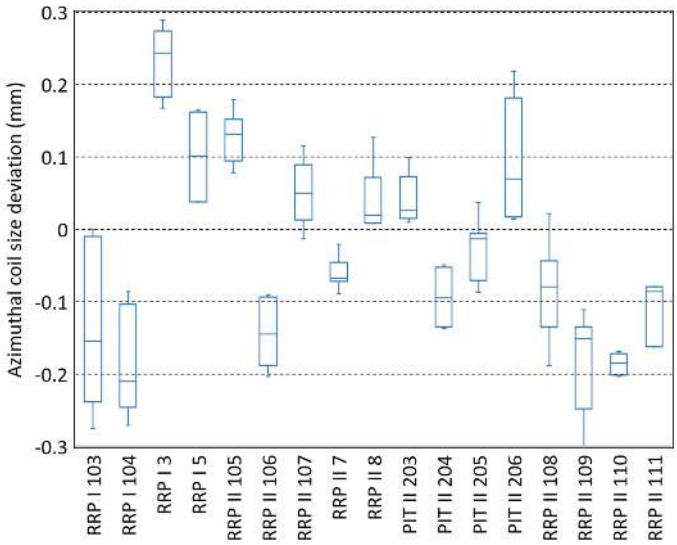

Fig. 4. Azimuthal coil size deviation (left + right mid-plane) with respect to nominal dimension for short model 1st (I) and 2nd (II) generation coils: from left to right, coils for MQXFS1-3-5-4.

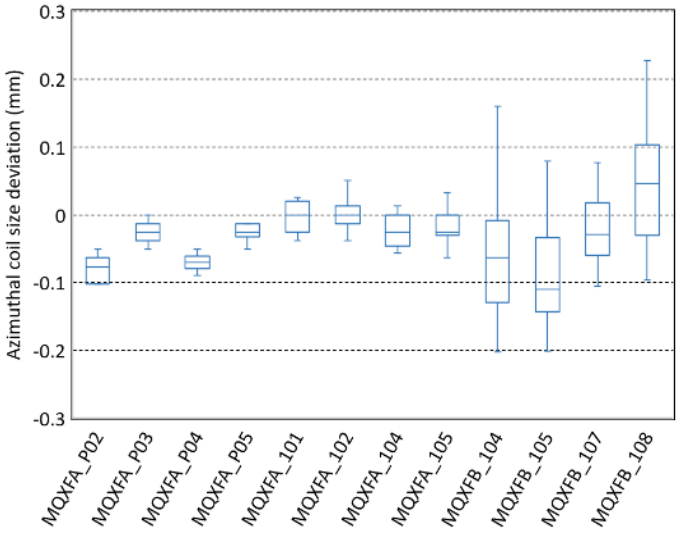

Fig. 5. Azimuthal coil size deviation (left + right mid-plane) with respect to nominal dimensions for prototype coils: from left to right, coils for MQXFAP1-2 and MQXFBP1.

For the short model coils, 7 cross-sections at a 150 mm distance along the coil straight section are analyzed, while for the MQXFA (MQXFB) the measurements are taken on respectively 11 (32) locations 420 (200) mm apart. In Fig. 4 and 5, the

azimuthal deviations (left + right mid-plane) for each of the tested coils with respect to nominal dimensions are given in the form of a box plot: the horizontal lines indicate the minimum, the 25% percentile, the median, the 75% percentile, and the maximum deviations. The short coils have a size variation along the length up to 0.250 mm, and a median value ranging from -0.200 to +0.250 mm. No significant difference is found between RRP of PIT coils, or between first and second generation coils. In the case of the prototype coils, the medians range between -0.100 and +0.050 mm, but MQXFA coils show a significant smaller variation along the axis with respect to MQXFB coils.

IV. Magnet Assembly and Loading

The measurements of the coil dimensions provide the inputs to define a shimming plan, the first step of the coil-pack assembly. In order to compensate for size deviations, coils are shimmed radially and/or on the mid-plane, so that the final outer radius of the four coils coincides. A 2D magnetic analysis is performed to determine the coil locations within the four quadrants to minimize the un-allowed harmonics. Then, the assembly of the MQXF structure, described in detailed in [18]-[21] and showed in Fig. 6, and its pre-load with water pressurized bladders are carried out.

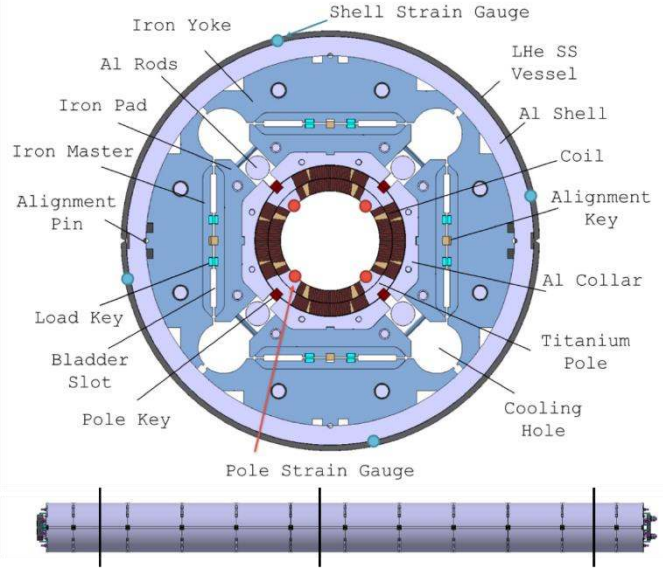

Fig. 6. MQXF cross-section (top), and side view of MQXFB (bottom). The red and blue markers (top) indicate the locations of the strain gauges on coils and shell, and the vertical lines (bottom) their longitudinal positions.

In Fig. 7, a summary of the pre-load of the tested MQXF magnets is depicted: the azimuthal stress measured on the coil is plotted as a function of the azimuthal stress measured on the shell [22], [23]. Data from all the magnets are compared with numerical computations simulating the case with full contact between collars and pole keys and the case without pole keys. For a given tension in the shell, the coil compression can be increased by applying a gap between the pole key and the collars, thus reducing the compressive force intercepted by the collars.

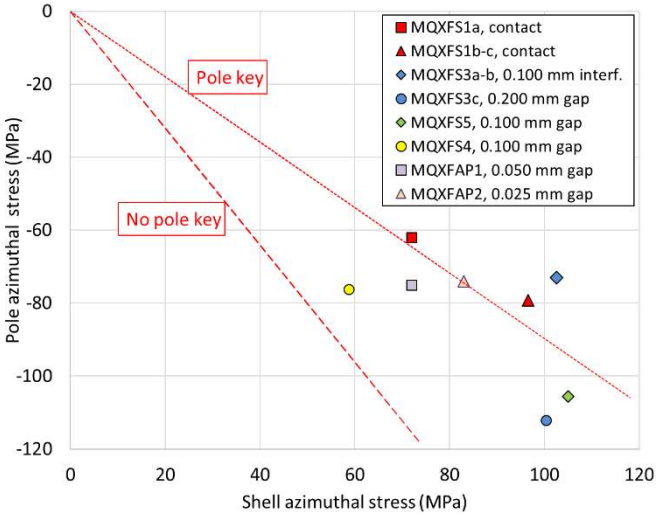

Fig. 7. Azimuthal stress measured in the winding pole vs. azimuthal stress measured in the aluminum shell, both at 293 K. The gaps/interferences in the legend are between collars and pole keys, per side. Data from tested magnets are compared with computed values considering the case with full contact between collars and pole keys and the case without pole keys.

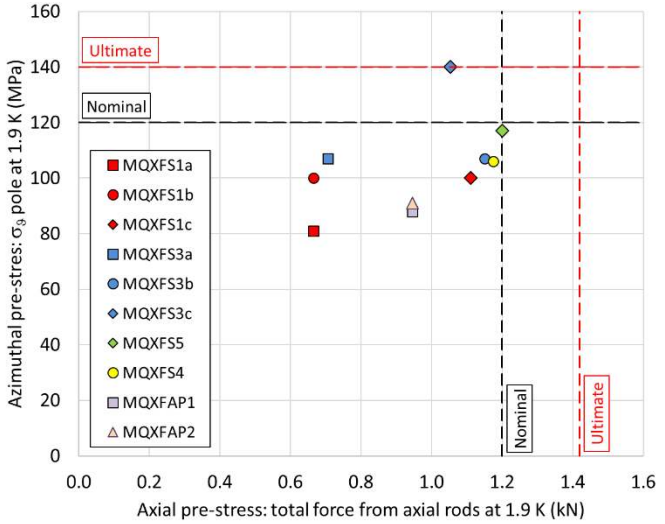

Fig. 8. Azimuthal stress measured in the winding pole vs. total longitudinal force applied by the axial load system, after cool-down. Data from tested magnets are compared to target values to (*y* axis) prevent azimuthal unloading of the coil and to (*x* axis) equal the longitudinal electro-magnetic forces.

Several configurations have been explored in the short models and the MQXFA prototypes, ranging from an interference of 0.100 mm in MQXFS3a-b to a gap of 0.200 mm in MQXFS3c, resulting in a coil pre-load varying from -60 MPa to -110 MPa. Measured data are consistent with the computations: the larger the pole key gap, the closer are the data to the "no pole key" computed line.

After cool-down, an increase of shell stress, caused by its high thermal contraction, produces an increase of coil azimuthal compression. The data for the tested magnets are shown in Fig. 8 (*y* axis) and compared with target values: the two horizontal lines indicate the levels of coil compression that, according to computations and strain gauge measurements [24], prevent at I_{nom} and I_{ult} an azimuthal unloading of the coil pole turns due to the electro-magnetic (e.m.) forces. In addition, the plot provides

the total longitudinal pre-load given to the coils by the axial support system, and compare it with the axial e.m. forces (see Table IV) at I_{nom} and I_{ult} (vertical lines). It can be noticed that after cool-down, a conservative approach with low pre-load was chosen for MQXFS1, and a progressive increase toward higher pre-loads was pursued in the following magnets. For the MQXFA prototypes, a low azimuthal and an intermediate axial pre-load were chosen.

TABLE IV
COIL AND MAGNET PARAMETERS

Parameter	Unit	
Coil clear aperture diameter	mm	150
Magnet (LHe vessel) outer diameter	mm	630
No. turns in layer 1/2 (octant)		22/28
Operational temperature T_{op}	K	1.9
Magnetic length (Q1-Q3)/(Q2)	M	4.20/7.15
Nominal gradient G_{nom}	T/m	132.6
Nominal current I_{nom}	kA	16.47
Nominal conductor peak field B_{op}	T	11.4
I_{nom} / I_{ss} at 1.9 K for RRP/PIT (specs.)	%	77/79
Ultimate gradient G_{ult}	T/m	143.2
Ultimate current I_{ult}	kA	17.89
Ultimate conductor peak field B_{ult}	T	12.3
I_{ult} / I_{ss} at 1.9 K for RRP/PIT (specs.)	%	84/86
Stored energy density at I_{nom} (Q1-Q3)/(Q2)	MJ/m	1.17
Differential inductance at I_{nom}	mH/m	8.21
Stored energy at I_{nom} (Q1-Q3)/(Q2)	MJ	4.91/8.37
F_x / F_y (per octant) at I_{nom}	MN/m	+2.47/ -3.48
F_ϑ layer1/layer2 (per octant)	MN/m	-1.84/-2.14
F_z (whole magnet) at I_{nom}	MN	1.17

V. QUENCH PERFORMANCE

Both short models and MQXFA prototypes test campaigns started with so-called single-coil tests, where individual coils were assembled inside an iron structure (so-called mirror configuration) without pre-load and powered at 1.9 K. Although not representative of the mechanical conditions of the full quadrupole magnets, the single coil configuration is characterized by a load-line comparable to the MQXF quadrupole magnet, and therefore it can provide an early feed-back on the coil design and fabrication process. The test of the first MQXFS coil (MQXFSM1) was carried out at FNAL in May 2015, while the test of the first MQXFA coil (MQXFAM1) was performed at BNL in December 2016. In both tests (Fig. 9) the coils passed the ultimate current and reached about 87% of I_{ss} at 1.9 K. After the single coil tests, four short model magnets (MQXFS1-3-5-4) and two MQXFA prototype magnets (MQXFAP1-2) have been powered. Coil parameters and loading conditions for these magnets can be found in Table III and Fig. 7 and Fig. 8. Their quench performance are provided in the next sub-sections, and compared with I_{nom}, I_{ult} and I_{ss}. The latter was evaluated by measurements of witness samples, that is strands extracted from the cables used to wind the coils, and reacted with the coils.

A. MQXFS1

The first short model magnet tested is MQXFS1. The test started at FNAL in March 2016 [25]-[27]. The magnet used first generation coils, with RRP 108/127 and 132/169 conductor, fabricated at FNAL and BNL (2 coils), and at CERN (2 coils). In term of pre-load, a conservative approach was adopted, with about -80 MPa on the coil after cool-down, and a longitudinal pre-load of about half of the axial e.m. force (see Fig. 8). The magnet had a first quench at 14.2 kA, reached I_{nom} in 8 quenches and I_{ult} in 16 quenches. At 4.5 K, MQXFS1 maintained the same quench current and after thermal cycle exhibited perfect memory.

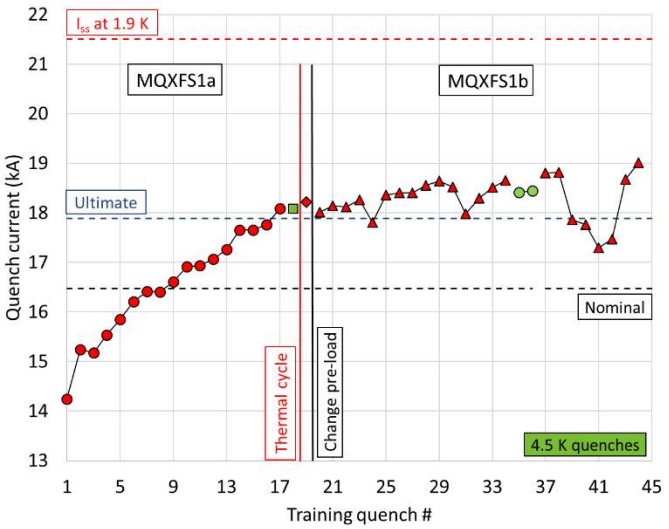

Fig. 10. Quench current of MQXFS1a-b. Ramps are at 20 A/s unless indicated. Data are compared to nominal, ultimate and short-sample current (estimated from witness samples).

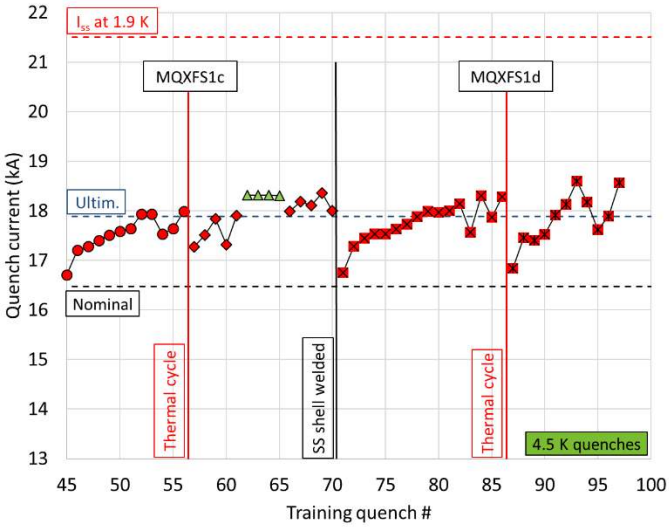

Fig. 11. Quench current of MQXFS1c-d. Ramps are at 20 A/s unless indicated. Data are compared to nominal, ultimate and short-sample current (estimated from witness samples).

Since the pole gauges clearly indicated unloading during powering, after the thermal cycle MQXFS1 was warmed-up, re-loaded to a higher azimuthal pre-load and tested at 1.9 K as MQXFS1b. Despite about 6 detraining quenches, the magnet

reached a maximum current of 19 kA, and demonstrated high temperature margin with 2 quenches at 4.2 K above $I_{ult.}$ The test of MQXFS1 continued with an increase of axial pre-load (MQXFS1c), followed by the welding of the stainless steel shell (MQXFS1d): in both cases, as shown in Fig, 11, it showed a loss of memory and about 5 de-training quenches, but it still managed to pass $I_{ult.}$.

B. MQXFS3

MQXFS3 was assembled with 2nd generation coils, fabricated at FNAL and BNL and at CERN with RRP 108/127, 132/196, and 144/169 conductor. It was tested at CERN in October 2016 [28]-[29].

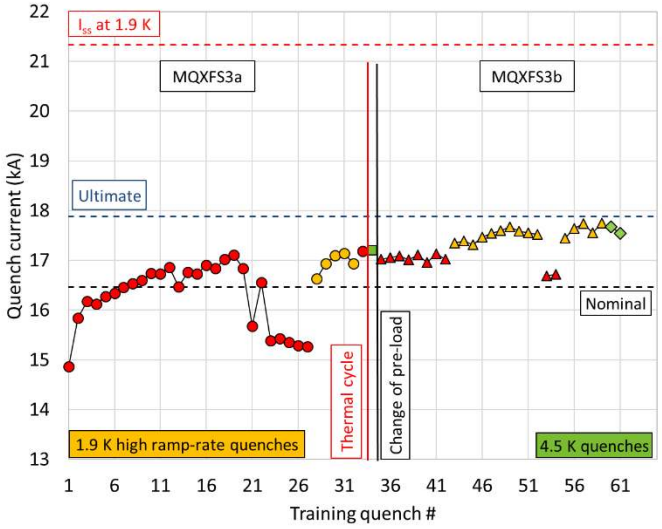

Fig. 12. Quench current of MQXFS3a-b. Ramps are at 20 A/s unless indicated. Data are compared to nominal, ultimate and short-sample current (estimated from witness samples).

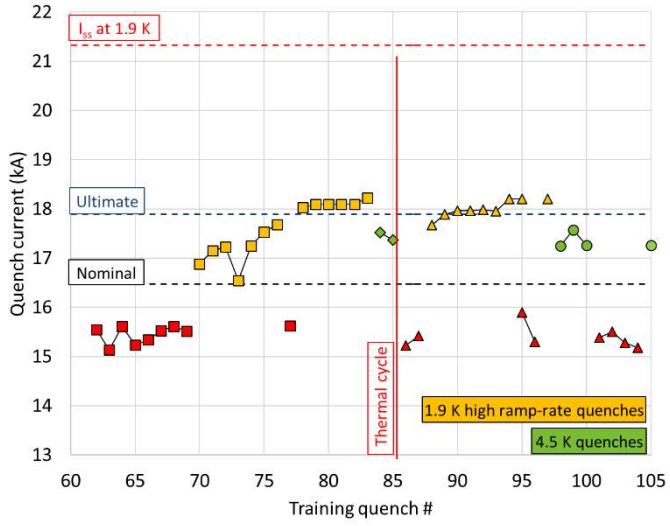

Fig. 13. Quench current of MQXFS3c. Ramps are at 20 A/s unless indicated. Data are compared to nominal, ultimate and short-sample current (estimated from witness samples).

As shown in Fig. 12, the training started at 14.9 kA, and I_{nom} was achieved in 7 quenches, but after quench #19 a progressive drop in current was recorded. The detraining quenches were all located in the lead end region of coil 7. The magnet managed to climb back to the original quench currents only by increasing the ramp-rates from 20 to 50-300 A/s. A similar behavior was observed also in MQXFS3b, where an increase of axial pre-load, aimed at addressing the issue in the end of coil 7, improved the quench level of the 20 A/s ramps; however, higher quench currents were reached only with increased ramp-rates or temperature. Such a behavior could be attributed to a strand self-field instability [30], possibly linked to a mechanical damage. It was therefore decided to disassemble MQXFS3b and replace coil 7 with a new coil (8). A visual inspection of the magnet components pointed out a major damage in the pole key, which in MQXFS3a was assembled with 0.100 mm interference to the collars.

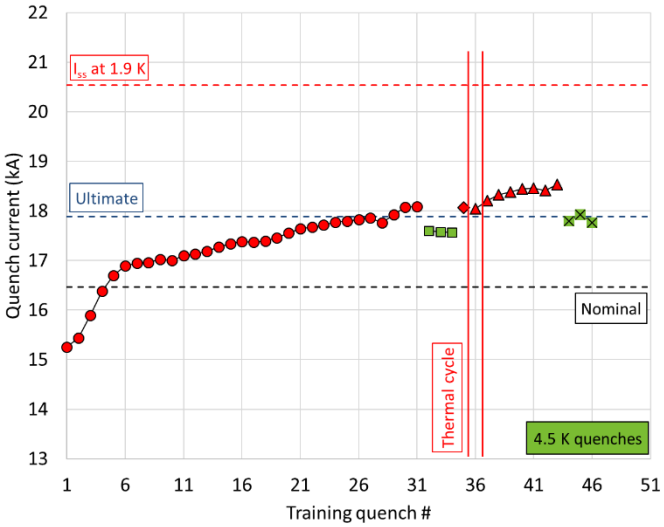

Fig. 14. Quench current of MQXFS5. Ramps are at 20 A/s unless indicated. Data are compared to nominal, ultimate and short-sample current (estimated from witness samples).

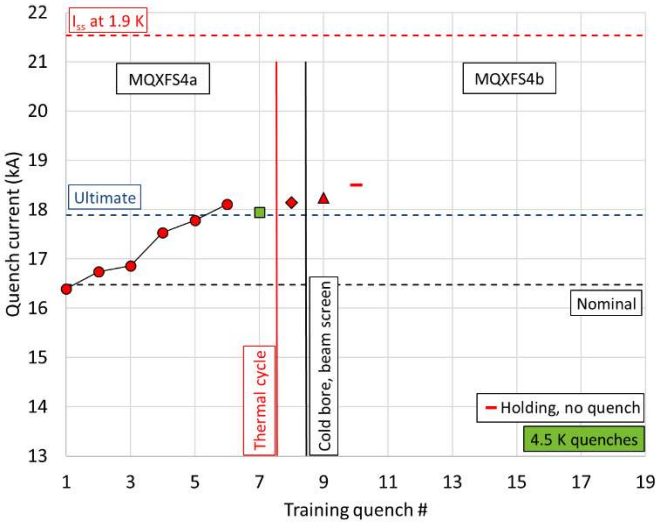

Fig. 15. Quench current of MQXFS4. Ramps are at 20 A/s unless indicated. Data are compared to nominal, ultimate and short-sample current (estimated from witness samples).

As a result, the magnet was reassembled with a 0.200 mm gap between collar and pole keys (see Fig. 7). In addition, the azimuthal pre-stress a 1.8 K was increased from -110 MPa to -140

MPa (see Fig. 8). The magnet, named MQXFS3c, behaved similarly as the previous ones, being limited at 20 A/s by an "old" coil (106).

C. MQXFS5 and MQXFS4

The following 2 magnets, MQXFS5 and MQXFS4, tested at CERN in July 2017 [28] and July 2018 [29], used both four uniform 2nd generation coils, the first with PIT 192 strand (without bundle barrier), and the second with RRP 108/127, all fabricated at CERN. Unlike MQXFS3a, they were assembled with gaps between collar and pole key (see Fig 7) and after cool-down they both had axial and azimuthal nominal pre-load (see Fig 8). The two magnet reached I_{ult} at 1.9 K and 4.2 K, with full memory (see Fig. 14 and Fig. 15).

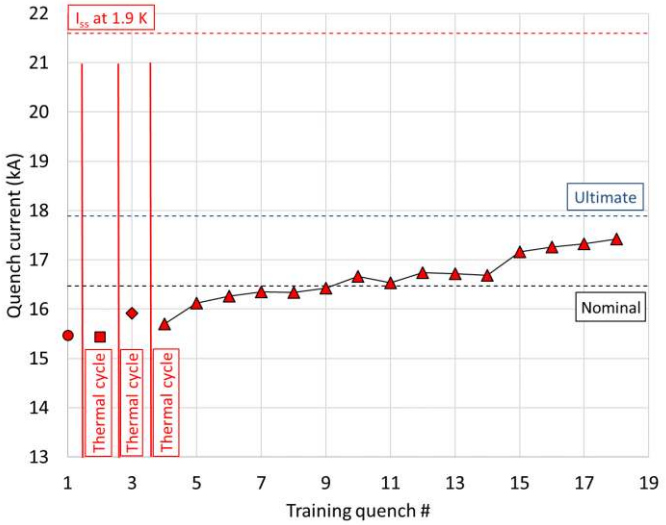

Fig. 16. Quench current of MQXFAP2. Ramps are at 20 A/s unless indicated. Data are compared to nominal, ultimate and short-sample current (estimated from witness samples).

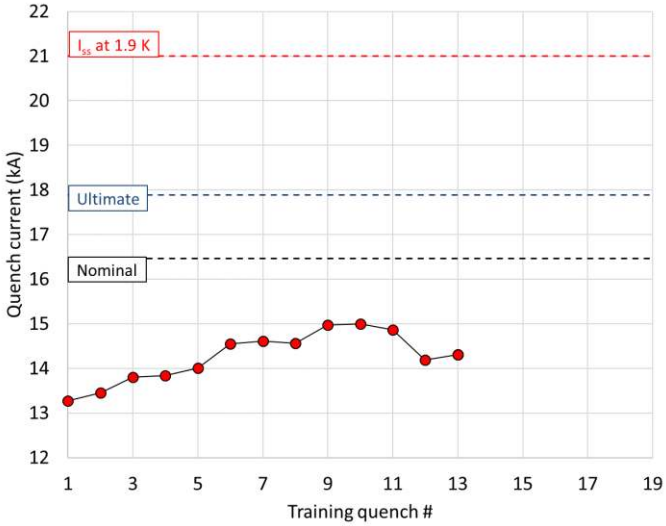

Fig. 17. Quench current of MQXFAP2. Ramps are at 20 A/s unless indicated. Data are compared to nominal, ultimate and short-sample current (estimated from witness samples).

After the first test, MQXFS4 was warmed up and a cold bore with the HL-LHC beam screen was inserted. After a first quench at 18.2 kA, 100 A higher than the last quench of MQXFS4a, the magnet was powered to 18.5 kA without quench.

D. MQXFAP1 and MQXFAP2

The first MQXFA prototype, still with 1st generation coils 4.0 m long, fabricated at FNAL and BNL with RRP 108/127 (1 coil), 132/169 (2 coils), and 144/169 (1 coil) conductor, was tested at BNL in August 2017 [31]. After a first quench at a current level (14.2 kA) comparable to the ones of the short models, the magnet went through 3 thermal cycles due to issues in the cryogenic system. The magnet was then trained up to a current of 17.4 kA, when an electrical short between quench heater and coil outer layer forced to stop the test and to warm-up the magnet.

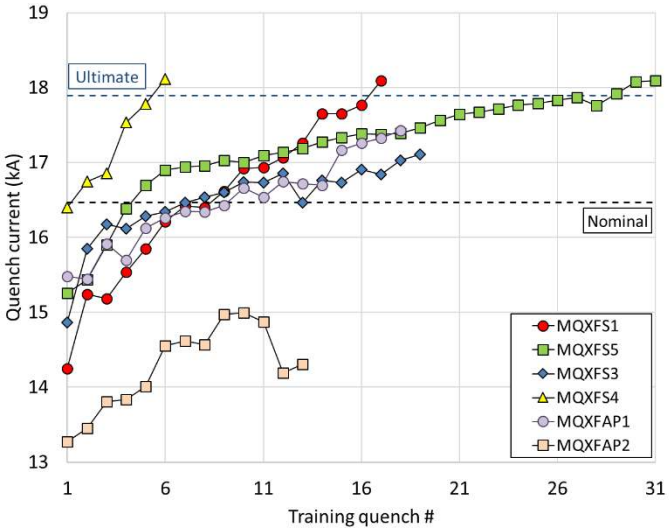

Fig. 18. Comparison of quench current during training of the fist thermal cycle of tested magnets, at 1.9 K and 20 A/s. Quenches of MQXFS3 are plotted only up to the maximum current before degradation. Data are compared to nominal, ultimate and short-sample current (estimated from witness samples).

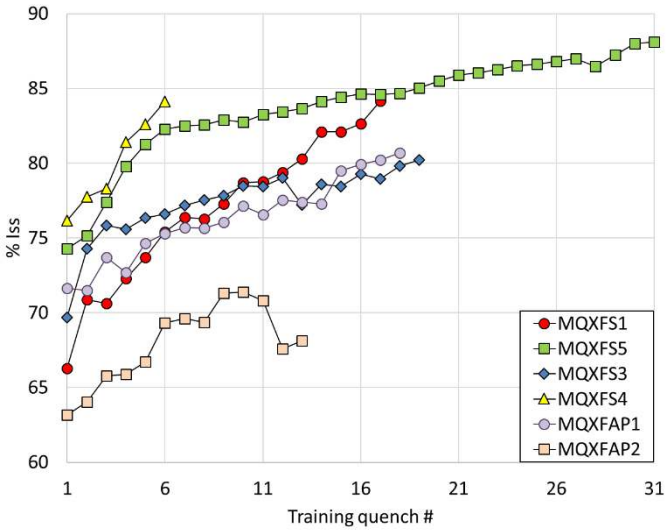

Fig. 19. Comparison of percent of I_{ss} of quenches during training of the fist thermal cycle of tested magnets, at 1.9 K and 20 A/s. Quenches of MQXFS3 are plotted only up to the maximum current before degradation.

The second prototype, MQXFAP2, started at BNL in September 2018. The magnet used 2nd generation coils, with RRP

108/127 conductor, fabricated at FNAL and BNL, and all 4.2 m long. The magnet had a first quench at 13.3 kA and reached 15 kA in 10 quenches, followed by detraining quenches. The test and the analysis is currently in progress.

E. Comparison of Training Performance

A comparisons between the magnets tested so far can be seen in. Fig. 18, where we plot the quench currents, and in Fig. 19, where the percentage of I_{ss} are given. In both cases, only the 1.9 K quenches of the first thermal cycle, obtained with a ramp-rate of 20 A/s, are shown. The quenches of MQXFS3 are plotted only up to the occurrence of the de-training in coil 7. It can be noticed that: 1) all magnet reached I_{nom}, while only 3 reached I_{ult}; 2) the first quench current ranges from 13.2 kA to 16.4 kA, and its percentage of short sample from 63% to 76%; 3) the number of quenches to reach I_{nom} varies from a maximum of 9 in MQXFAP1 to a minimum of minimum of 1 in MQXFS4; 4) there is not a clear correlation between magnet pre-load and quench performance.

VI. Conclusions and Future Plans

The development of the MQXF quadrupole magnets for the HL-LHC project is moving towards the completion of the short model phase and is advancing in the prototype one. So far, 31 coils have been, or are being, tested. A large variation of pre-load conditions and pole key to collar interfaces have been explored. All magnets reached the nominal current. A coil degradation and an electrical short prevented respectively MQXFS3 and MQXAP1 limited the magnet performance. At the time of the submission of this paper, the test of the second prototype is in progress and the assembly of MQXFBP1 has started.

References

[1] "The High Luminosity Large Hadron Collider", edited by O. Brüning and L. Rossi, *World Scientific*, October 2015.

[2] E. Todesco, *et al.,* "Design Studies for the Low-Beta Quadrupoles for the LHC Luminosity Upgrade," *IEEE Trans. Appl. Supercond.*, vol. 23 no. 3, pp. 4002405, June 2013.

[3] E. Todesco, *et al.,* "A first baseline for the magnets in the high luminosity LHC insertion regions," *IEEE Trans. Appl. Supercond.*, vol. 24 no. 3, pp. 4003305, June 2014.

[4] P. Ferracin, *et al.,* "Magnet Design of the 150 mm Aperture Low-β Quadrupoles for the High Luminosity LHC," *IEEE Trans. Appl. Supercond.*, vol. 24 no. 3, pp. 4002306, June 2014.

[5] P. Ferracin, *et al.,* "Development of MQXF: The Nb_3Sn Low-β Quadrupole for the HiLumi LHC", *IEEE Trans. Appl. Supercond.*, vol. 26 no. 4, pp. 4000207, June 2016.

[6] E. Todesco, *et al.,* "Progress on HL-LHC Nb3Sn Magnets", *IEEE Trans. Appl. Supercond.,* vol. 28 no. 4, pp. 4008809, June 2018.

[7] S. A. Gourlay, *et al.*, "Magnet R&D for the US LHC Accelerator Research Program", *IEEE Trans. Appl. Supercond.*, vol. 16, no. 2, pp. 324-327, June 2006.

[8] B. Bordini, *et al.*, "The Bundle-Barrier PIT Wire Developed for the Hi-Lumi LHC Project", *IEEE Trans. Appl. Supercond.*, vol. 27 no. 4, pp. 6000706, June 2017.

[9] E. Rochepault, *et al.*, "Dimensional Changes of Nb_3Sn Rutherford Cables During Heat Treatment", *IEEE Trans. Appl. Supercond.*, vol. 26 no. 4, pp. 4802605, June 2016.

[10] L. Bottura and B. Bordini, "J_c *(B, T, ε)* Parameterization for the ITER Nb_3Sn Production," *IEEE Trans. Appl. Supercond.*, vol. 19 no. 3, pp. 1521-1529, June 2009.

[11] S. Izquierdo Bermudez, *et al.*, "Second-Generation Coil Design of the Nb_3Sn low-β Quadrupole for the High Luminosity LHC", vol. 26 no. 4, pp. 4001105, June 2016.

[12] E. F. Holik, *et al.*, "Fabrication and Analysis of 150-mm-Aperture Nb_3Sn MQXF Coils", *IEEE Trans. Appl. Supercond.*, vol. 26 no. 4, pp. 4000907, June 2016.

[13] F. Lackner, *et al.*, "Status of the Long MQXFB Nb_3Sn Coil Prototype Production for the HiLumi LHC", *IEEE Trans. Appl. Supercond.*, vol. 27 no. 4, pp. 4002605, June 2017.

[14] M. Yu, *et al.*, "Coil End Parts Development Using BEND and Design for MQXF by LARP", *IEEE Trans. Appl. Supercond.*, vol. 27 no. 4, pp. 4000105, June 2017.

[15] E. F. Holik, *et al.*, "Fabrication of First 4-m Coils for the LARP MQXFA Quadrupole and Assembly in Mirror Structure", *IEEE Trans. Appl. Supercond.*, vol. 27 no. 4, pp. 4003605, June 2017.

[16] F. Lackner, *et al.*, "Fabrication of the 7.3-m-Long Coils for the Prototype of MQXFB, the Nb_3Sn Low-b Quadrupole Magnet for the HiLumi LHC", *IEEE Trans. Appl. Supercond.*, vol. 28 no. 3, pp. 4005605, April 2018.

[17] J. Ferradas Troitino, *et al.*, "Applied Metrology in the Production of Superconducting Model Magnets for Particle Accelerators", *IEEE Trans. Appl. Supercond.*, vol. 28 no. 3, pp. 4002106, April 2018.

[18] G. Vallone, *et al.*, "Mechanical Performance of Short Models for MQXF, the Nb_3Sn Low-β Quadrupole for the Hi-Lumi LHC", *IEEE Trans. Appl. Supercond.*, vol. 27 no. 4, pp. 4002906, June 2017.

[19] H. Pang, *et al.*, "Mechanical Design Studies of the MQXF Long Model Quadrupole for the HiLumi LHC", *IEEE Trans. Appl. Supercond.*, *IEEE Trans. Appl. Supercond.*, vol. 27 no. 4, pp. 4004105, June 2017.

[20] G. Vallone, *et al.*, "Mechanical Design Analysis of MQXFB, the 7.2-m-Long Low-β Quadrupole for the High-Luminosity LHC Upgrade", *IEEE Trans. Appl. Supercond.*, vol. 28 no. 3, pp. 4003705, April 2018.

[21] G. Vallone, *et al.*, " Assembly of MQXFBP1, Mechanical Model of the 7.2 m Long Low-β Quadrupole for the High Luminosity LHC Upgrade", *IEEE Trans. Appl. Supercond.*, submitted for publication.

[22] G. Vallone, *et al.*, "Mechanical Analysis of the Short Model Magnets for the Nb_3Sn Low-β Quadrupole MQXF", *IEEE Trans. Appl. Supercond.*, vol. 28 no. 3, pp. 4003106, April 2018.

[23] G. Vallone, *et al.*, "Summary of the Mechanical Performances of the 1.5 Long Models of the Nb3Sn Low-β Quadrupole MQXF", *IEEE Trans. Appl. Supercond.*, submitted for publication.

[24] G. Vallone and P. Ferracin, "Modeling Coil-Pole Debonding in Nb_3Sn Superconducting Magnets for Particle Accelerators", *IEEE Trans. Appl. Supercond.*, vol. 27 no. 8, pp. 4004611, December 2017.

[25] G. Chlachidze, *et al.*, "Performance of the First Short Model 150-mm-Aperture Nb_3Sn Quadrupole MQXFS for the High-Luminosity LHC Upgrade", *IEEE Trans. Appl. Supercond.*, vol. 27 no. 4, pp. 4000205, June 2017.

[26] T. Strauss, *et al.*, "Quench Location in the LARP MQXFS1 Prototype", *IEEE Trans. Appl. Supercond.*, vol. 28 no. 3, pp. 4001604, April 2018.

[27] S. Stoynev, *et al.*, "Summary of Test Results of MQXFS1—The First Short Model 150 mm Aperture Nb3Sn Quadrupole for the High-Luminosity LHC Upgrade", *IEEE Trans. Appl. Supercond.*, vol. 28 no. 3, pp. 4001705, April 2018.

[28] H. Bajas, *et al.*, "Test Result of the Short Models MQXFS3 and MQXFS5 for the HL-LHC Upgrade", *IEEE Trans. Appl. Supercond.*, vol. 28 no. 3, pp. 4007006, April 2018.

[29] G. J. Mangiarotti, *et al.*, "Test Results of the CERN HL-LHC low-beta Quadrupole short Models MQXFS3c and MQXFS4", *IEEE Trans. Appl. Supercond.*, submitted for publication.

[30] B. Bordini, L. Bottura, L. Oberli, L. Rossi, "Impact of the Residual Resistivity Ratio on the Stability of Nb_3Sn Magnets ", *IEEE Trans. Appl. Supercond.*, vol. 28 no. 3, pp. 4007006, April 2018.

[31] V. Marinozzi, *et al.*, "Analysis of the short-to-ground event in the LARP-AUP MQXFAP1 magnet, and its implication on the production and tests of the series magnets", *IEEE Trans. Appl. Supercond.*, submitted for publication.